Climate Dynamics (2006) 26: 329–348
DOI 10.1007/s00382-005-0084-6

Eric Guilyardi

El Niño–mean state–seasonal cycle interactions in a multi-model ensemble

Received: 24 May 2005 / Accepted: 18 September 2005 / Published online: 19 November 2005

Abstract The modelled El Niño–mean state–seasonal cycle interactions in 23 coupled ocean–atmosphere GCMs, including the recent IPCC AR4 models, are assessed and compared to observations and theory. The models show a clear improvement over previous generations in simulating the tropical Pacific climatology. Systematic biases still include too strong mean and seasonal cycle of trade winds. El Niño amplitude is shown to be an inverse function of the mean trade winds in agreement with the observed shift of 1976 and with theoretical studies. El Niño amplitude is further shown to be an inverse function of the relative strength of the seasonal cycle. When most of the energy is within the seasonal cycle, little is left for inter-annual signals and vice versa. An interannual coupling strength (ICS) is defined and its relation with the modelled El Niño frequency is compared to that predicted by theoretical models. An assessment of the modelled El Niño in term of SST mode (S-mode) or thermocline mode (T-mode) shows that most models are locked into a S-mode and that only a few models exhibit a hybrid mode, like in observations. It is concluded that several basic El Niño–mean state–seasonal cycle relationships proposed by either theory or analysis of observations seem to be reproduced by CGCMs. This is especially true for the amplitude of El Niño and is less clear for its frequency. Most of these relationships, first established for the pre-industrial control simulations, hold for the double and quadruple CO_2 stabilized scenarios. The models that exhibit the largest El Niño amplitude change in these greenhouse gas (GHG) increase scenarios are those that exhibit a mode change towards a T-mode (either from S-mode to hybrid or hybrid to T-mode). This follows the observed 1976 climate shift in the tropical Pacific, and supports the—still debated—finding of studies that associated this shift to increased GHGs. In many respects, these models are also among those that best simulate the tropical Pacific climatology (ECHAM5/MPI-OM, GFDL-CM2.0, GFDL-CM2.1, MRI-CGM2.3.2, UKMO-HadCM3). Results from this large subset of models suggest the likelihood of increased El Niño amplitude in a warmer climate, though there is considerable spread of El Niño behaviour among the models and the changes in the subsurface thermocline properties that may be important for El Niño change could not be assessed. There are no clear indications of an El Niño frequency change with increased GHG.

E. Guilyardi (✉)
Laboratoire des Sciences du Climat et de l'Environnement (IPSL/LSCE), Gif-sur-Yvette, France
E-mail: Eric.Guilyardi@cea.fr

E. Guilyardi
CGAM, Department of Meteorology, University of Reading, Reading, UK

1 Introduction

El Niño events represent regular major disruptions of the annual cycle of the tropical ocean–atmosphere system in the Pacific, with consequences on the whole planet. Predicting El Niño occurrence and amplitude, both on the seasonal time scale and for the next century is a key societal need. Simple El Niño models and observation networks were instrumental in clarifying the basic mechanisms and feedbacks at play during an El Niño event [see the recent review of Wang and Picaut (2004)].

Nevertheless, the diversity of observed events suggested that (1) the precise sequence and relative importance of the mechanisms and feedbacks responsible for a particular event varies and (2) the interaction with the basic state and seasonal cycle could play a key role. Indeed the mechanisms that drive the mean state and seasonal cycle in the tropical Pacific (Gill mechanism or Bjerknes feedbacks for instance) also operate during El Niño (Dijkstra and Neelin 1995; Chang 1996; Nigam

and Chao 1996). More generally, the tropical Pacific climatology is the result of similar physical mechanisms that operate on a variety of space and time scales that cannot be separated. Nevertheless, and even though an El Niño event is defined as an anomaly to the seasonal cycle, very few studies analysed the role of this seasonal cycle (this is most likely due to the fact that earlier El Niño models had their seasonal cycle and mean state specified).

Jin et al. (1994), Tziperman et al. (1994, 1997) and Chang et al. (1995) have discussed the irregularity of El Niño in the context of simplified ocean–atmosphere models and argued that it is consistent with a low-order chaotic system interacting with the seasonal cycle. In comparing simulations of glacial and interglacial climates, Clement et al. (1999, 2000) have shown that El Niño interacting with a modified seasonal cycle lead to a mean tropical change. Chang et al. (1995) underline dual roles of the seasonal cycle in El Niño variability: it introduces a degree a regularity in the El Niño cycle by producing an annual phase locking and it generates irregularity via non-linear interactions. By performing a wavelet analysis of observations, Gu and Philander (1995) suggested that the amplitude of the seasonal cycle was related to the El Niño activity.

The impact of the mean state (also studied as decadal variability) was both prompted by El Niño paleoclimate studies (Tudhope et al. 2001; Cobb et al. 2003) and the observed 1976 climate shift in the tropical Pacific (Guilderson and Schrag 1998; Urban et al. 2000; Trenberth and Hurrell 1994). The change of observed El Niño characteristics before and after this date was attributed to the change of mean winds by several authors (Wang and An 2002; Karspeck and Cane 2002). Fedorov and Philander (2001) proposed a theoretical study relating El Niño frequency and growth rate to the mean wind and mean thermocline depth in tropical Pacific. They identified two unstable modes that could lead to El Niño events with distinct characteristics. Knutson and Manabe (1998) went further in proposing to attribute the post-1976 warming to the increase of greenhouse gases (GHG) in the atmosphere, also pointing out that the mechanisms involved during these longer time scale were similar to those involved during El Niño events.

A key aspect of the links between El Niño and the mean state and the seasonal cycle is the east–west contrast in the tropical Pacific. Even though both contribute to establish the zonal SST gradient central to the equatorial dynamics, the balance of mechanisms for these two regions, broadly separated by the date line, are very different. For instance, Chang (1996) has shown that the east Pacific strong annual cycle was mostly driven by a strong ocean–atmosphere coupling, whereas the west Pacific seasonal cycle was mostly forced by the seasonal changes in the solar radiation. In terms of El Niño dynamics, previous work describe two types of modes that can give rise to El Niño (Neelin et al. 1998; Fedorov and Philander 2001; Burgers and van Oldenborgh 2003; Wang and Picaut 2004): the S-mode resulting from local SST–winds interactions in the central-east Pacific, implying surface east to west propagation of SST anomalies and low amplitude events with a 2–3 years frequency, as evidenced in observations for the pre-1976 period (also called by some authors SST mode, local mode or slow mode) and the T-mode, resulting from remote winds–thermocline feedbacks involving the west Pacific, implying subsurface west to east propagation and large amplitude events with 4–5 years frequency, as evidenced in observations for the post-1976 period with the 1982/83 and 1997/98 events (also found in the literature as thermocline mode, fast mode, remote mode or delayed oscillator mode). Fedorov and Philander (2001) have shown that the T-mode required weaker trade winds and deeper thermocline when compared to the S-mode.

Thanks to constant improvements of the physics, the numerics and the resolution of their components, as well as available computer power, coupled ocean–atmosphere General Circulation Models (CGCM) have recently emerged both as analysis and predictive tools for El Niño (Delecluse et al. 1998; Latif et al. 2001; Davey et al. 2001; AchutaRao and Sperber 2002; Guilyardi et al. 2004). The quality of their modelled climate now makes it possible to assess their El Niño properties in the light of theoretical results. Most prominently, the multi-model database recently established for the Fourth Assessment Report of the Intergovernmental Panel on Climate Change (IPCC AR4) provides an unprecedented collection of long integrations of quality models, and will be used in this study.

Previous single CGCM studies analysing El Niño behaviour show a diversity of responses to increasing GHG (Meehl et al. 1993, 2005; Tett 1995; Timmermann et al. 1999; Collins 2000a, b; Zelle et al. 2005). Multi-model analysis of El Niño in a warmer climate (Collins and the CMIP Modelling Groups 2005; van Oldenborgh et al. 2005; Merryfield 2005) proposed to classify models as a function of their El Niño skill to compute a weighted probability of El Niño change. These last two multi-model studies broadly concluded that no change in El Niño characteristics had the highest probability.

The goals of this paper are to, first, use the newly establish IPCC AR4 database to assess the relationships between the modelled El Niño characteristics and the modelled mean state and seasonal cycle in stabilized integrations, hence providing detailed feedbacks to modelling groups, second, assess how these relations fit with existing El Niño theory, and third, assess if/how these relations can evolve in a stable warmer climate (doubled or quadrupled CO_2), as evidenced in past climates.

The paper is organized as follows: Sect. 2 presents the multi-model ensemble and the output used, Sect. 3 explores the impact of the mean state and the seasonal cycle on the modelled El Niño, Sect. 4 classifies the models into El Niño modes and Sect. 5 discusses the major findings.

Table 1 The models used in the present study, including, configurations (near the equator) and number of years of simulations

Model	Institution	Atmosphere resolution	Ocean resolution	Length picntrl	Length 1pctto2x	Length 1pctto4x
CCSM3	NCAR (USA)	T85L26	1.125°×0.27°L40	230	150	n/a
CGCM3.1(T47)	CCCMA (Canada)	T47L31	1.85°×1.85°L29	500	150	150
CNRM-CM3	Meteo-France/CNRM (France)	T63L45	2°×0.5°L31	390	100	110
CSIRO-Mk3.0	CSIRO (Australia)	T63L18	1.875°×0.84°L31	380	10	n/a
ECHAM5/MPI-OM	MPI-M (Germany)	T63L31	1.5°×0.5°L40	332	100	81
FGOALS-g1.0	LASG/IAP (China)	T42L26	1°×1°L33	150	80	n/a
GFDL-CM2.0	GFDL (USA)	2.5°×2°L24	1°×0.33°L50	500	100	160
GFDL-CM2.1	GFDL (USA)	2.5°×2°L24	1°×0.33°L50	500	150	160
GISS-AOM	NASA/GISS (USA)	4°×3°L12	4°×3°L16	251	n/a	n/a
GISS-EH	NASA/GISS (USA)	5°×4°L20	2°×2°L16	500	80	150
GISS-ER	NASA/GISS (USA)	5°×4°L20	5°×4°L13	400	100	n/a
INM-CM3	INM (Russia)	5°×4°L21	2.5°×2°L33	330	n/a	n/a
IPSL-CM4	IPSL (France)	2.5°×3.75°L19	2°×0.5°L31	230	80	n/a
MIROC3.2(hires)	CCSR/NIES/FRCGC (Japan)	T106L56	0.28°×0.1875°L47	100	10	n/a
MIROC3.2(medres)	CCSR/NIES/FRCGC (Japan)	T42L20	1.4°×0.5°L43	500	100	150
MRI-CGM2.3.2	MRI (Japan)	T42L30	2.5°×0.5°L23	350	150	150
PCM	NCAR (USA)	T42L18	0.66°×0.5°L32	350	96	90
UKMO-HadCM3	HadleyCentre (UK)	3.75°×2.5°L19	1.25°×1.25°L20	341	10	n/a
UKMO-HadGEM1	HadleyCentre (UK)	1.875°×1.25°L38	1°×0.33°L40	80	10	n/a
SINTEX T30	IPSL/INGV (France,Italy)	T30L19	2°×0.5°L31	200	n/a	n/a
SINTEX T106	INGV/IPSL (Italy,France)	T106L19	2°×0.5°L31	100	n/a	n/a
SINTEX T106mod	IPSL/INGV (France,Italy)	T106L19	2°×0.5°L31	100	n/a	n/a
HadOPA	CGAM/IPSL (UK,France)	3.75°×2.5°L19	2°×0.5°L31	100	n/a	n/a

The only flux corrected model is MRI-CGM2.3.2

2 Multi-model ensemble

Table 1 presents the models used in this study. The first 19 models are taken from the IPCC AR4 database (managed by PCMDI), which collects the result of many years of dedicated work from modelling groups around the world. Model references can be obtained from the IPCC web site.[1] The last four models are not part of the IPCC AR4 but were analysed in the Guilyardi et al. (2004) modular intercomparison where ocean and atmosphere components were swapped. They are added here to increase the number of models to 23. For all models, the sea surface temperature (SST) and zonal wind stress (τ_x) were analysed (IPCC variable names: ts—tas for HadCM3/picntrl—and tauu). In this study, we do not wish to add a degree of complexity by analysing transient scenarios. We therefore chose to study the pre-industrial control (picntrl) and the *stabilized* $2\times CO_2$ and $4\times CO_2$ scenarios (years after year 70 for 1pctto2×[2] and years after year 140 for 1pctto4×[3]). Because of this restriction, some scenarios data are missing (either not available on the IPCC data server or time serie too short) and we did not replace them by another scenario (unless otherwise specified). Note that: (1) the first (''run1'') or longest ensemble member was used for each scenario, (2) if at least 10 years of stabilised scenario were available, the seasonal cycle was computed, (3) inter-annual statistics were performed only if at least a 80 years of data were available (but for HadGEM1); experience has shown that El Niño statistics computed on shorter time series are misleading for some models as they can be biased by lower frequency variability, (4) the last four models were integrated with constant present-day GHG concentrations; it was checked with several ''stabilized @2000'' IPCC integrations that their basic El Niño properties did not differ significantly from those of the corresponding picntrl integration (not shown). The stabilized 1pctto2× and 1pctto4× choice represents a best case scenario for pulling out El Niño change. In a transient forcing experiment (which is what the real system is), these changes would be more difficult to ascertain when forcing is gradually changing and inherent decadal variability is also a large factor (Trenberth and Hurrell 1994).

The observation–based analysis used for reference are: HadISST1.1 (1900–2000), Rayner et al. (2003) or NCEP (1948–2004) for SST and NCEP (1948–2004) for τ_x.

These observations represent a 20c3m ''scenario'' rather than a picntrl and in terms of mean state, the picntrl simulation should be compared to the earlier part of the observations although the quality of the data in the tropical Pacific region before 1950 is poor. We therefore present observation results for the full record and for before and after the 1976 climate shift.

[1] http://www-pcmdi.llnl.gov/ipcc/model_documentation/ipcc_model_documentation.php

[2] 1pctto2x scenario: CO_2 is increased by 1% per year from 1860 until doubling, 70 years after, and then held constant.

[3] 1pctto4x scenario: CO_2 is increased by 1% per year from 1860 until quadrupling, 140 years after, and then held constant.

3 Relating El Niño characteristics, the mean state and the seasonal cycle

3.1 Modelled El Niño characteristics

El Niño characteristics in GCMs can be diagnosed in many different ways. Here, we start with basic and widely used ones and then refine the analysis in the next section. We define the amplitude of El Niño as the monthly standard deviation of the SST anomaly in the Niño3 region (5°S to 5°N–150°W to 90°W) (Table 2). The dominant frequency(ies) is(are) defined as the significant peak(s) in the normalized spectra of Niño3 SST anomaly (as in Guilyardi et al. 2004) (Fig. 1).

A wavelet analysis of SST observations since 1860 shows that the 5.3*y* peak is for the recent period (after 1976, as will be discussed in Sect. 4), and the 3.5*y* peak for the preceding period (Fedorov and Philander 2001). Note that if the wavelet analysis is applied to the southern ocean index (SOI), this change of frequency is less clear (G. van Oldenborgh, personal communication, 2005).

Modelled pre-industrial control El Niño amplitudes fall into four categories (Table 2): those with almost no inter-annual signal (GISS-AOM and GISS-ER), those with about half the value of the observed variability of about 0.9°C (CGCM3.1(T47), and the two MIROC3.2), those within ±20% of observation (CCSM3, CSIRO-Mk3.0, GFDL-CM2.0, GISS-EH, INM-CM3, IPSL-CM4, MRI-CGM2.3.2, PCM, UKMO-HadCM3, UKMO-HadGEM1, SINTEX T30, SINTEX T106, and SINTEX T106 mod) and those with a larger- to much larger-than-observed variability (CNRM-CM3, ECHAM5/MPI-OM, FGOAL-g1.0, GFDL-CM2.1 and HadOPA). In the remainder of the paper, the models of the first category (GISS-AOM and GISS-ER) will not be discussed, even though present in the tables and figures.

Among the models that fall in the last two categories, the modelled El Niño frequency (Fig. 1) can be organized in those with a higher-than observed frequency (CCSM3, CSIRO-Mk3.0, IPSL-CM4, MRI-CGM2.3.2, SINTEX T30, SINTEX T106 mod) with a subset of those that exhibit too regular events (as evidence by a single sharp peak: CCSM3 and IPSL-CM4), and those with a broadly correct dominant frequency (CNRM-CM3, ECHAM5/MPI-OM, FGOALS-g1.0, GFDL-CM2.0, GFDL-CM2.1, GISS-EH, INM-CM3, PCM, UKMO-HadCM3, UKMO-HadGEM1, SINTEX T106 and HadOPA), with again a too regular subset (CNRM-CM3, FGOALS-g1.0, UKMO-HadGEM1 and HadOPA).

In the stabilized 2×CO_2, 7 out of 12 models exhibit a statistically significant change of El Niño amplitude when compared to the pre-industrial controls (Table 2).

Table 2 Main El Niño, mean state and seasonal cycle properties of the models (pre-industrial control)

Model	Code	ElNiño amplitude	SST (°C) Niño3	τ_x(Pa) Niño4	SCRS (%)	ICS	2×CO_2 (%)	4×CO_2 (%)
Observed		0.88 ± 0.02	25.87 ± 0.05	−0.029 ± 0.006	31	8.7		
Obs 1948–1975		0.71 ± 0.04	25.72 ± 0.49	−0.032 ± 0.003		10.4		
Obs 1976–2004		0.94 ± 0.36	26.03 ± 0.06	−0.026 ± 0.000		8.5		
CCSM3	A	0.78 ± 0.04	25.29 ± 0.08	−0.038 ± 0.000	20	6.1	−13	
CGCM3.1(T47)	B	0.42 ± 0.03	24.63 ± 0.15	−0.045 ± 0.002	41	11.6	+5	+2
CNRM-CM3	C	1.66 ± 0.21	23.43 ± 0.06	−0.026 ± 0.000	3	6.3	+1	**+7**
CSIRO-Mk3.0	D	0.90 ± 0.17	24.34 ± 0.23	−0.034 ± 0.000	20	7.8		
ECHAM5/MPI-OM	E	1.16 ± 0.09	25.16 ± 0.06	−0.034 ± 0.001	13	7.3	**+29**	**+31**
FGOALS-g1.0	F	1.93 ± 0.34	26.57 ± 0.16	−0.028 ± 0.001	0	6.6	**−27**	
GFDL-CM2.0	G	0.75 ± 0.19	24.74 ± 0.15	−0.043 ± 0.000	37	8.8	**+20**	**+25**
GFDL-CM2.1	H	1.32 ± 0.08	24.98 ± 0.14	−0.044 ± 0.000	12	12.8	+2	**−18**
GISS-AOM	I	0.17 ± 0.03	27.07 ± 0.01	−0.036 ± 0.000	45	17		
GISS-EH	J	0.86 ± 0.13	24.53 ± 0.13	−0.037 ± 0.001	24	0.8	**−5**	
GISS-ER	K	0.24 ± 0.01	28.16 ± 0.03	−0.026 ± 0.001	22	2.2	−21	+8
INM-CM3	L	0.92 ± 0.10	24.15 ± 0.09	−0.025 ± 0.001	23	6.2		
IPSL-CM4	M	1.00 ± 0.02	26.28 ± 0.08	−0.026 ± 0.000	13	5.9	**−16**	
MIROC3.2(hires)	N	0.35 ± 0.01	25.46 ± 0.14	−0.042 ± 0.002	86	15.4		
MIROC3.2(medres)	O	0.44 ± 0.11	24.81 ± 0.03	−0.040 ± 0.000	60	10.7	+5	+2
MRI-CGM2.3.2	P	0.70 ± 0.05	25.04 ± 0.04	−0.045 ± 0.000	35	16	**+34**	**+77**
PCM	Q	0.89 ± 0.19	24.23 ± 0.11	−0.034 ± 0.001	11	6.1	**−8**	**−13**
UKMO-HadCM3	R	0.77 ± 0.09	25.58 ± 0.07	−0.045 ± 0.001	13	10.3		
UKMO-HadGEM1	S	0.68 ± 0.17	23.69 ± 0.12	−0.064 ± 0.001	28	8.9		
SINTEXT30	T	0.61 ± 0.09	25.90 ± 0.08	−0.041 ± 0.001	13	8.5		
SINTEXT106	U	0.74 ± 0.07	26.27 ± 0.16	−0.035 ± 0.002	5	7.0		
SINTEXT106mod	V	0.67 ± 0.06	26.84 ± 0.25	−0.041 ± 0.002	8	6.6		
HadOPA	W	1.67 ± 0.14	27.46 ± 0.36	−0.035 ± 0.001	5	7.5		

CSRS is the seasonal cycle relative strength (in %), ICS the summer interannual coupling strength (in 10^{-3} Pa/C). The El Niño amplitude change to doubling and quadrupling of CO_2 (when compared to picntrl) are shown in the last two columns. The El Niño amplitude is defined as the standard deviation of SST in the Nino3 region. Errors were estimated with a moving block bootstrap to account for serial correlation (windows: El Niño period of Fig. 1 for standard deviation and 10 months for means). The amplitude change values underlined are significant at the 5% level

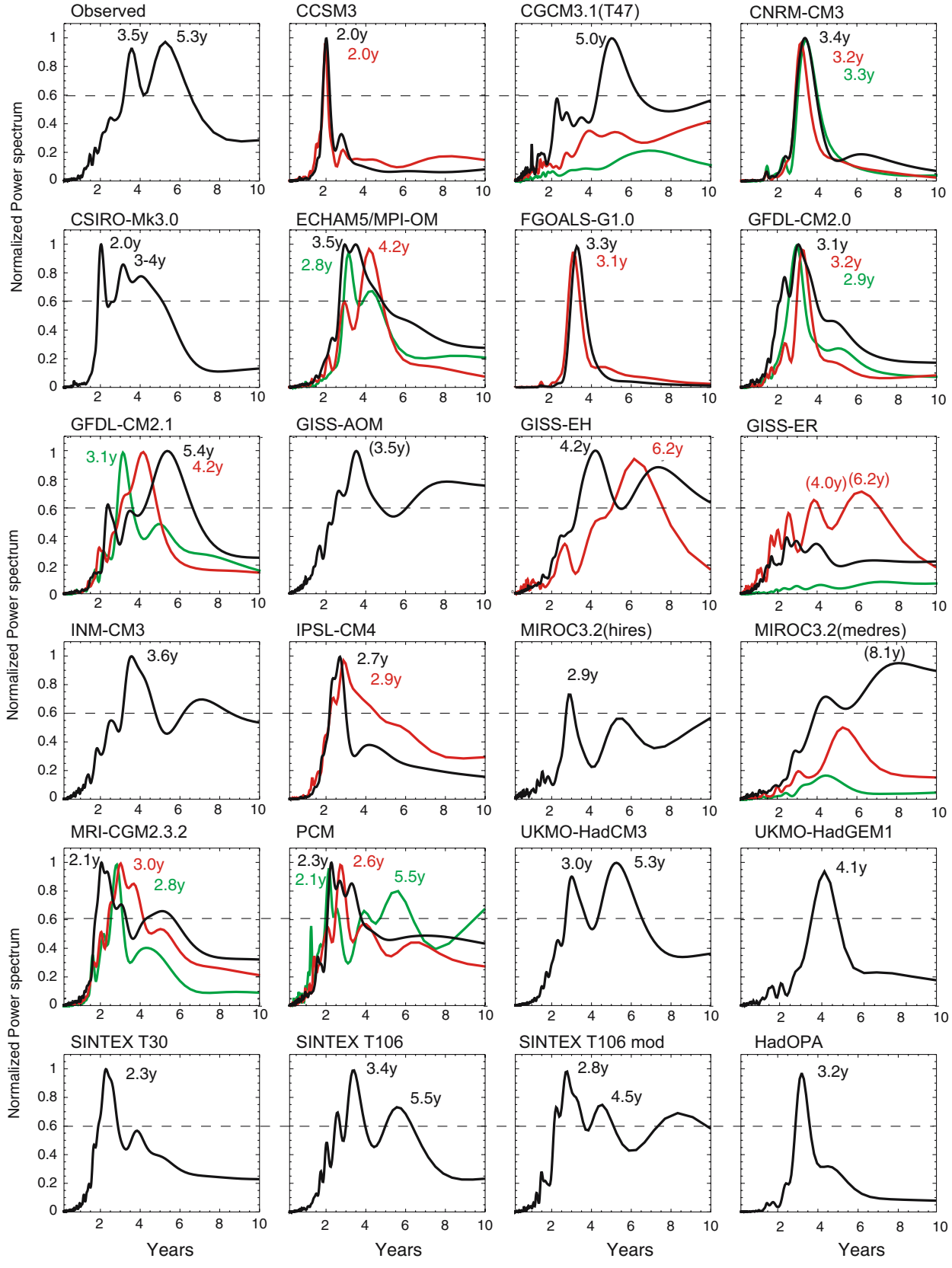

Fig. 1 Normalized power spectra of Niño3 SSTA for the 23 models studied, together with the available scenarios. Observation are for the HadISST1.1 dataset, years 1900–2000. Models colour code: *black* picntrl, *red* 1pctto2x (after stabilization), *green* 1pctto4x (after stabilization). Spectral peaks exceeding 0.6 are significant

Four models evolve towards an El Niño amplitude reduced down to −27% (CCSM3, IPSL-CM4, FGOALS-g1.0), while the three others evolve towards an amplitude increased up to +34% (GFDL-CM2.0, ECHAM5/MPI-OM, MRI-CGM2.3.2). In the stabilized 4×CO_2, six out of eight models exhibit a statistically significant change of amplitude when compared to the pre-industrial controls (Table 2). Two show a decrease of amplitude down to −18% (GFDL-CM2.1 and PCM) and four show an increase up to +77% (GFDL-CM2.0, ECHAM5/MPI-OM, MRI-CGM2.3.2).

For the category two and three of amplitude, the change of dominant frequency (Fig. 1), if any, are only significant for GFDL-CM2.1 (towards higher frequency), GISS-EH (towards lower frequency), IPSL-CM4 (broadening of peak) and MRI-CGM2.3.2 (towards lower frequency).

This initial analysis shows a wide range of El Niño behaviour for pre-industrial control simulations and no model agreement on El Niño evolution in stabilized warmer climates. We will now assess how these differences can be related to the modelled mean state and/or seasonal cycle.

Even though the analysis techniques are different, the El Niño properties described for the pictrnl simulations broadly agree with those described by AchutaRao and Sperber (2005) and Merryfield (2005) for pre-industrial controls and by van Oldenborgh et al. (2005) for the climate for the twentieth century (20c3m) simulations (exceptions are: GFDL-CM2.0 and MIROC3.2(medres) which seem to have stronger El Niño amplitude events in 20c3m when compared to pictrnl).

3.2 Relations with the mean state

The mean Niño4 region (5°S to 5°S–160°E to 150°W) τ_x is shown as a function of mean Niño3 SST in Fig. 2. The reason for choosing these specific regions will become clear in next section and using other equatorial regions does not change the basic properties discussed. For each model, a line connects the three scenarios (when available).

In terms of east equatorial SST, most models (picntrl) tend to be on the cold side, with a few extreme case (more than 1.5°C colder than mean observations for the period before 1976: CNRM-CM3, UKMO-HadGEM1, INM-CM3, PCM, CSIRO-Mk3.0). Some models are too warm by more than 1.5°C (HadOPA, GISS-ER). Most models have larger trade winds than observed (up to 50%), with one extreme case (+100% for UKMO-HadGEM1). Some models have weaker-than-observed trade winds, closer to recent observed period than to a picntrl (CNRN-CM3, IPSL-CM4, FGOAL-g1.0).

All models show a SST warming of 1–2°C in the stabilized 1pctto2x, associated with a slight reduction of the trade winds (about 10%) for most, and from 2 to almost 6°C in the stabilized 1pctto4x, with again a

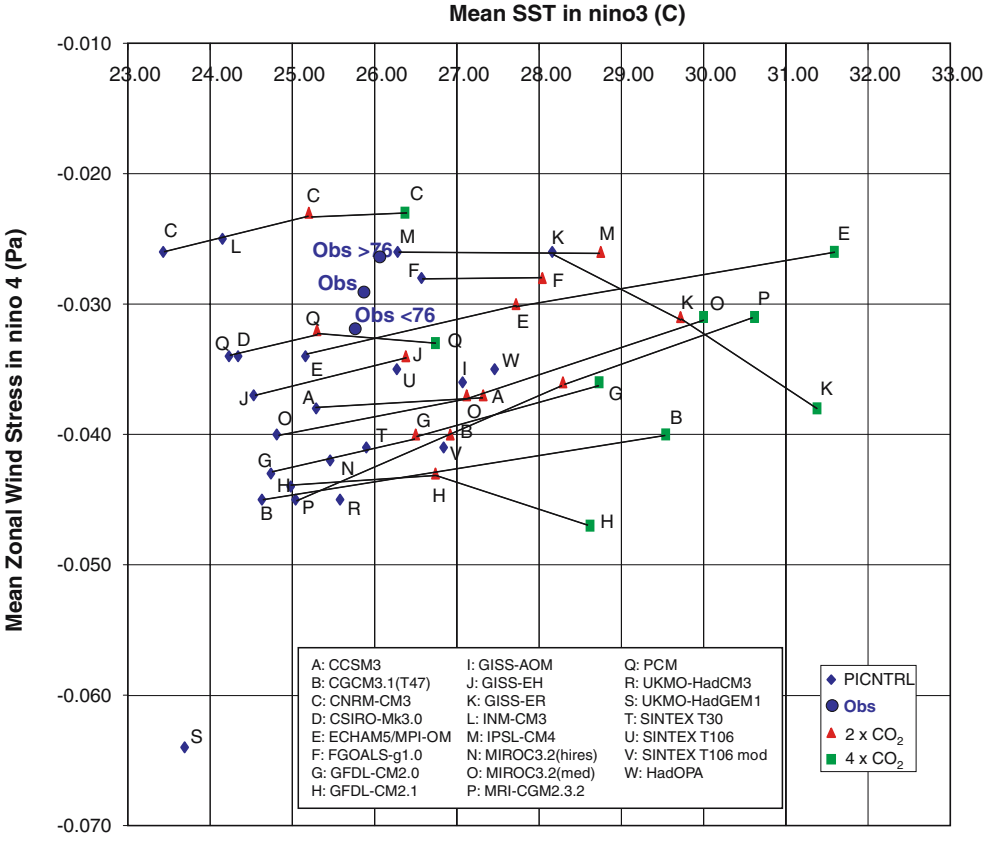

Fig. 2 Scatter plot of mean Niño4 τ_x as a function of mean Niño3 SST. *Black diamonds* picntrl, *red triangles* 1pctto2x (after stabilization), *green squares* 1pctto4x (after stabilization). The *blue circles* represent observations for the 1948–2001 period, and the values before and after 1976. *Letters* correspond to model codes in Table 2

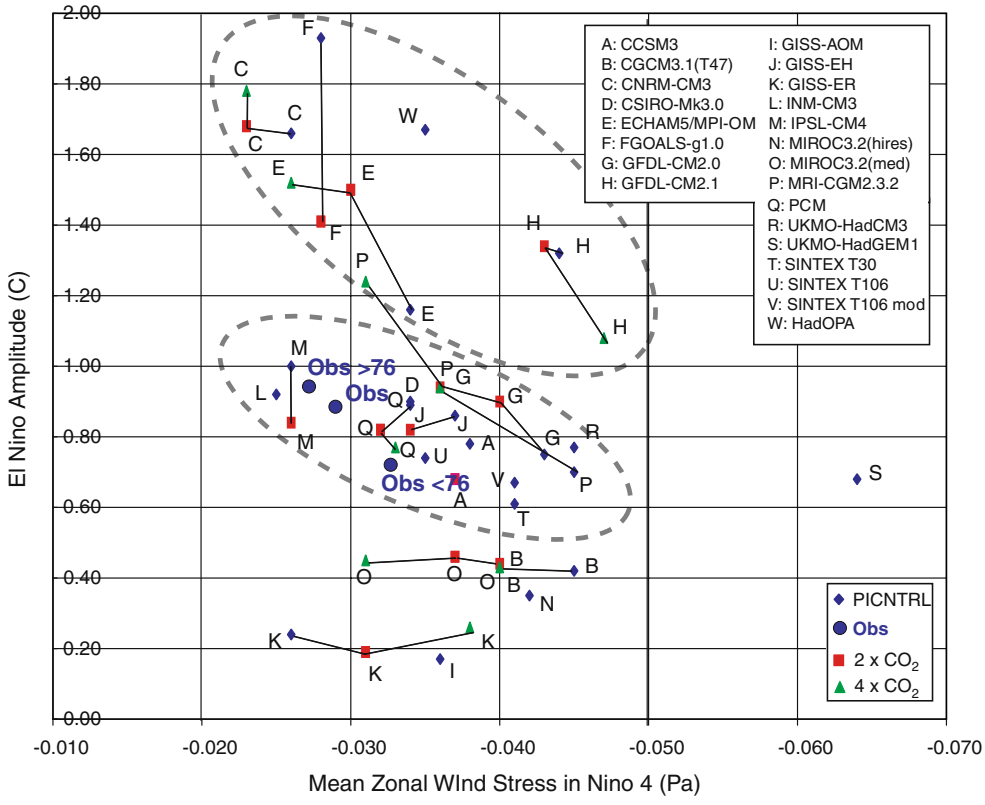

Fig. 3 Scatter plot of El Niño amplitude as a function of mean Niño4 τ_x. *Black diamonds* picntrl, *red squares* 1pctto2x (after stabilization), *green triangles* 1pctto4x (after stabilization). The *blue circles* represent observations for the 1948–2001 period, and the values before and after 1976. *Letters* correspond to model codes in Table 2

similar reduction in the trade winds for most. The SST response to CO_2 increase seems linear for most models (i.e. quadrupling doubles the signal of doubling). The wind response linearity is less systematic as a few models exhibit some sort of saturation, or even an increase of mean when comparing 1pctto4x to 1pctto2x (CNRM-CM3, PCM, GFDL-CM2.1).

Figure 3 presents the El Niño amplitude as a function of the mean Niño4 τ_x. For El Niño amplitude larger than 0.5°C, two groups can be distinguished: one around observations and one for larger amplitude El Niño models. For both groups, models with larger El Niño amplitude are also models with a weaker mean τ_x in Niño4, a relation also suggested by the comparison of the pre- and post-1976 observations and theoretical studies (Wang and An 2002). By using a linear stability analysis approach in a simple model, Fedorov and Philander (2001) also related mean properties of the tropical Pacific to El Niño characteristics. Besides mean winds, they also used the mean thermocline depth. Unfortunately, picntrl thermocline depth values were not available for enough models at time of analysis and it is difficult to compare with their results at this point. In addition, they provide a growth rate of the perturbation which does not necessarily relate to the El Niño amplitude presented here, owing the non-linearities of the systems modelled. Only one model (MRI-GCM2.3.2, flux corrected) changes group during the CO_2 increase.

No clear relation between mean Niño3 SST and El Niño characteristics could be established.

3.3 Relations with the seasonal cycle

The seasonal cycle in the equatorial tropical Pacific is first diagnosed as a Gill-like response by relating the Niño4 τ_x to the Niño3 SST (Fig. 4). This captures a large part of the mechanisms at play in driving the seasonal cycle in this region, which are also involved in an El Niño event (either re-enforced or missing).

In the observations, the annual cycle features three phases: (1) the spring (MAM) relaxation when the Niño3 SST reaches a maximum of 28°C and τ_x a minimum, (2) the summer (JJA) and autumn (SON) upwelling when the Niño3 SST decreases to 25°C and τ_x increases, and (3) the winter (DJF) τ_x maximum. Note that even though the forcing is semi-annual, the response is annual (Li and Philander 1996).

The models picntrl simulations exhibit a diversity of behaviours. A number of models have the correct three phases of the observed seasonal cycle (correct shape and relative position of seasons) with nonetheless a too marked semi-annual cycle (CGCM3.1(T47), CNRM-CM3, ECHAM5/MPI-OM, GFDL-CM2.0, GFDL-CM2.1, INM-CM3, IPSL-CM4, MRI-CGM2.3.2, UKMO-HadCM3, UKMO-HadGEM1, SINTEX models, HadOPA). Among these models, a striking feature of many is the much too strong amplitude of the τ_x seasonal cycle (exceptions are ECHAM5/MPI-OM, IPSL-CM4, UKMO-HadCM3 and HadOPA). Other models do not exhibit the spring τ_x relaxation, key to the seasonal phase locking of the El Niño cycle (CCSM3, CSIRO-Mk3.0, GISS-EH, PCM). Interestingly, the two

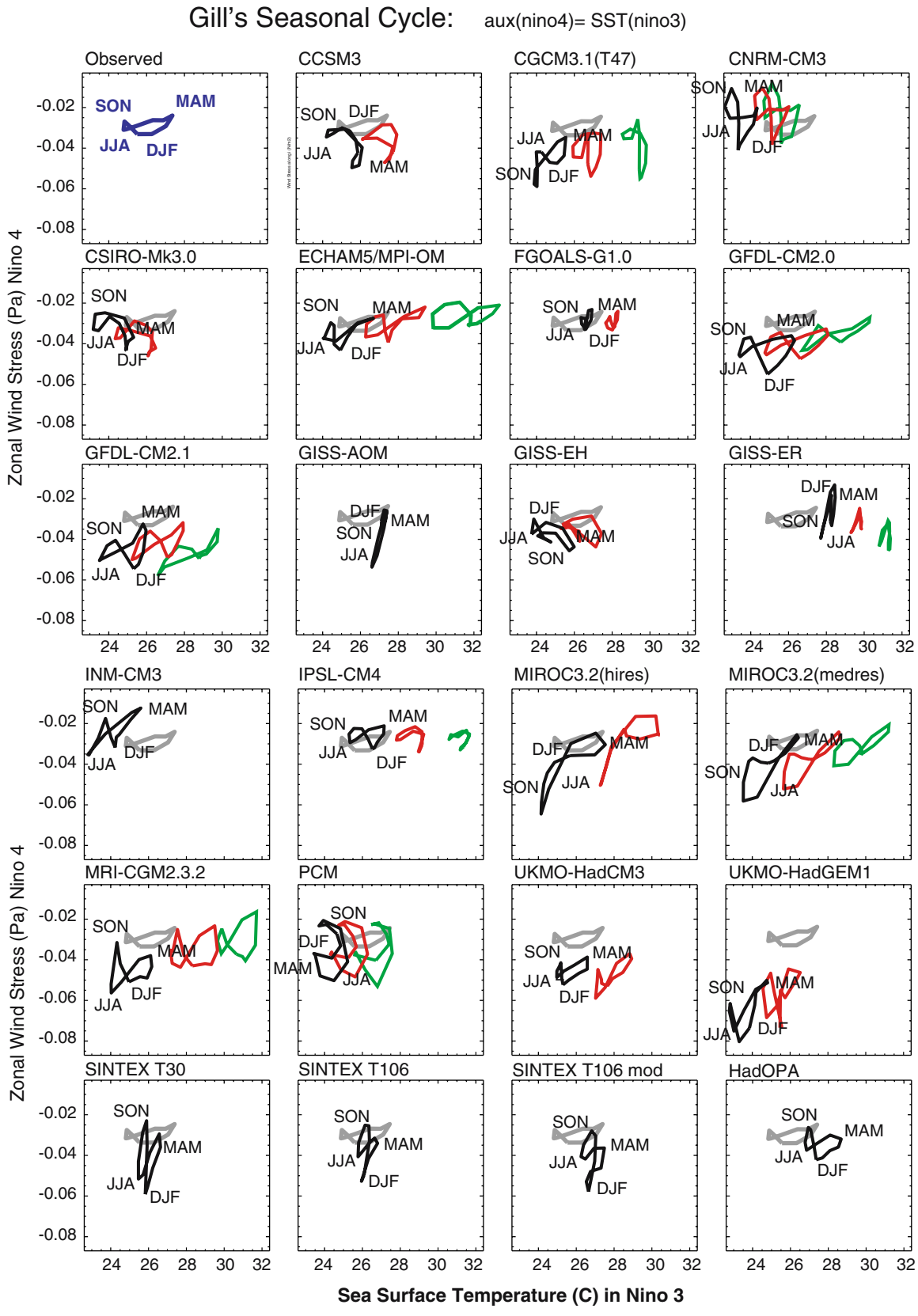

Fig. 4 Gill-like seasonal cycle for observations and for the models as represent by Niño4 zonal wind stress (τ_x) as a function of Niño3 SST. *Black* picntrl, *red* 1pctto2x (after stabilization), *green* 1pctto4x (after stabilization). Observed seasonal cycle is reproduced in *grey* for comparison. The position of the four seasons: MAM, JJA, SOM, DJF is shown for the picntrl simulations

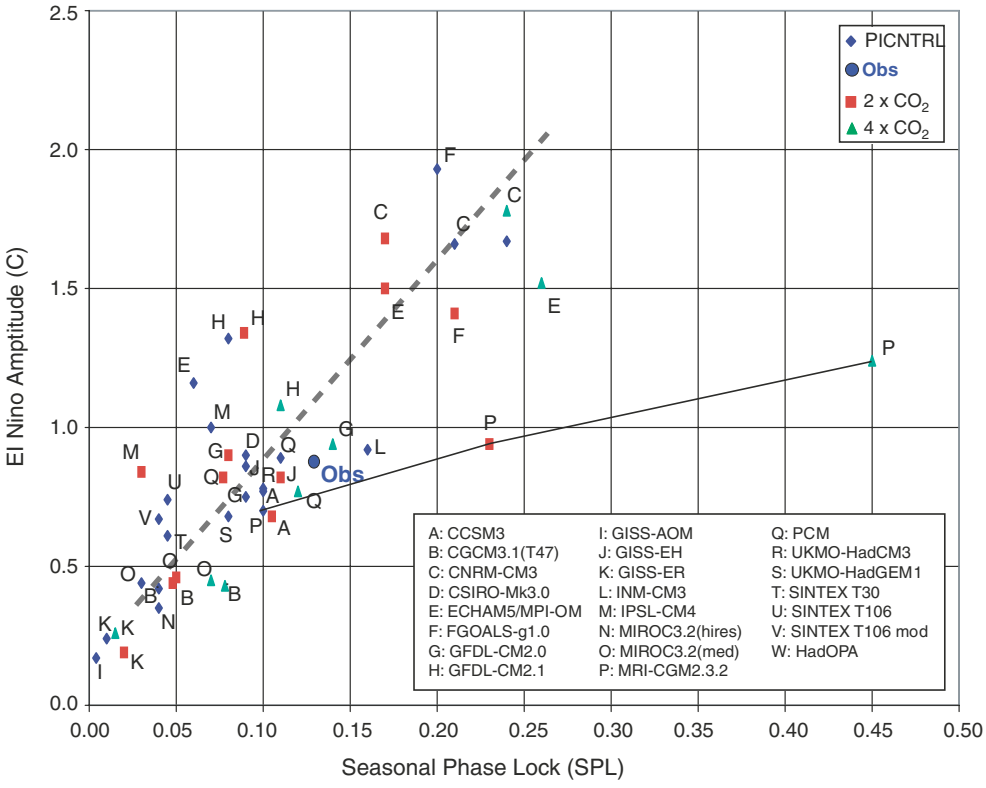

Fig. 5 El Niño amplitude as a function of the seasonal phase lock (*SPL*, see text for definition) and linear fit (*thick dashed line*, excluding the MRI-GCM2.3.2 model which is flux-corrected)

models that were discarded from the analysis as having no El Niño variability (GISS-AOM and GISS-ER) have very peculiar behaviour, with almost no seasonal cycle in SST and a large one in τ_x. Two models have an exceptionally large seasonal cycle in both SST and τ_x (the 2 MIROCS3.2) whereas another one has a very small seasonal cycle (FGOALS-g1.0).

In the 1pctto2x and 1pctto4x scenarios, the shape and errors of the seasonal cycle are mostly retained, but for some models that show some saturation of the maximum SST (CGCM3.1(T47), IPSL-CM4).

As a caveat, Burgers and van Oldenborgh (2003) and van Oldenborgh et al. (2005) have shown that fitting CGCM outputs to the actual mechanism proposed by Gill can be tricky and/or model dependent. Here the simple fixed-region Gill-type relation is chosen as a basic seasonal cycle diagnostic. Other regions were used to compute the relations presented here (like Niño3.4 SST) and this did not modify the results discussed above.

To examine in more details the impact of a relaxation in the seasonal cycle, a seasonal phase lock (SPL) index is computed as the annual amplitude of the monthly stratified standard deviation of Niño3 SSTA. A weak SPL will mean that the seasonal cycle does not offer a relaxation time for El Niño to develop (via Bjerknes feedbacks) whereas a large SPL will offer opportunities for El Niño development. This SPL does not offer information about the *timing* of the relaxation per se, although for observations and most models this occurs in the spring (Fig. 4). Not surprisingly, the modelled El Niño amplitude has an almost linear relationship with the SPL index (Fig. 5), indicating the key role of a seasonal relaxation of the winds to allow large El Niño event to develop. Interestingly, the monthly flux-corrected MRI-GCM2.3.2 model scenario do not fall on the El Niño/SPL relationship of the other models.

To further quantify the relationship between the seasonal cycle and the amplitude of El Niño in the models, a spectral analysis of the *full* Niño3 monthly SST time serie is performed (Fig. 6). The percentage of total spectral energy due to the annual and semi-annual cycles is also indicated (and reported in Table 2). In the observations, this percentage represents 31% of the total energy (mostly due the the annual cycle as the semi-annual is very small), leaving 69% to the inter-annual signal. In the models, this percentage, which measures the relative strength of the seasonal cycle, varies from 0% (FGOALS-g1.0) to 86% (MIROC3.2-hires). Most of the models do not have enough energy in the seasonal cycle, although a few models get the correct seasonal cycle relative strength (values between 20 and 40%: CCSM3, CGCM3.1(T47), CSIRO-Mk3.0, GFDL-CM2.0, GISS-EH, INM-CM3, MRI-CGM2.3.2 and UKMO-HadGEM1). Again, these values do not vary significantly in the scenario simulations, but for a few exceptions (increase for GFDL-CM2.1 and PCM and decrease for MRI-CGM2.3.2).

Figure 7 present El Niño amplitude as a function of the relative strength of the seasonal cycle as defined above. This analysis reveals that the amplitude of El Niño is an inverse function of the strength of the seasonal cycle as shown in observations (Gu and Philander

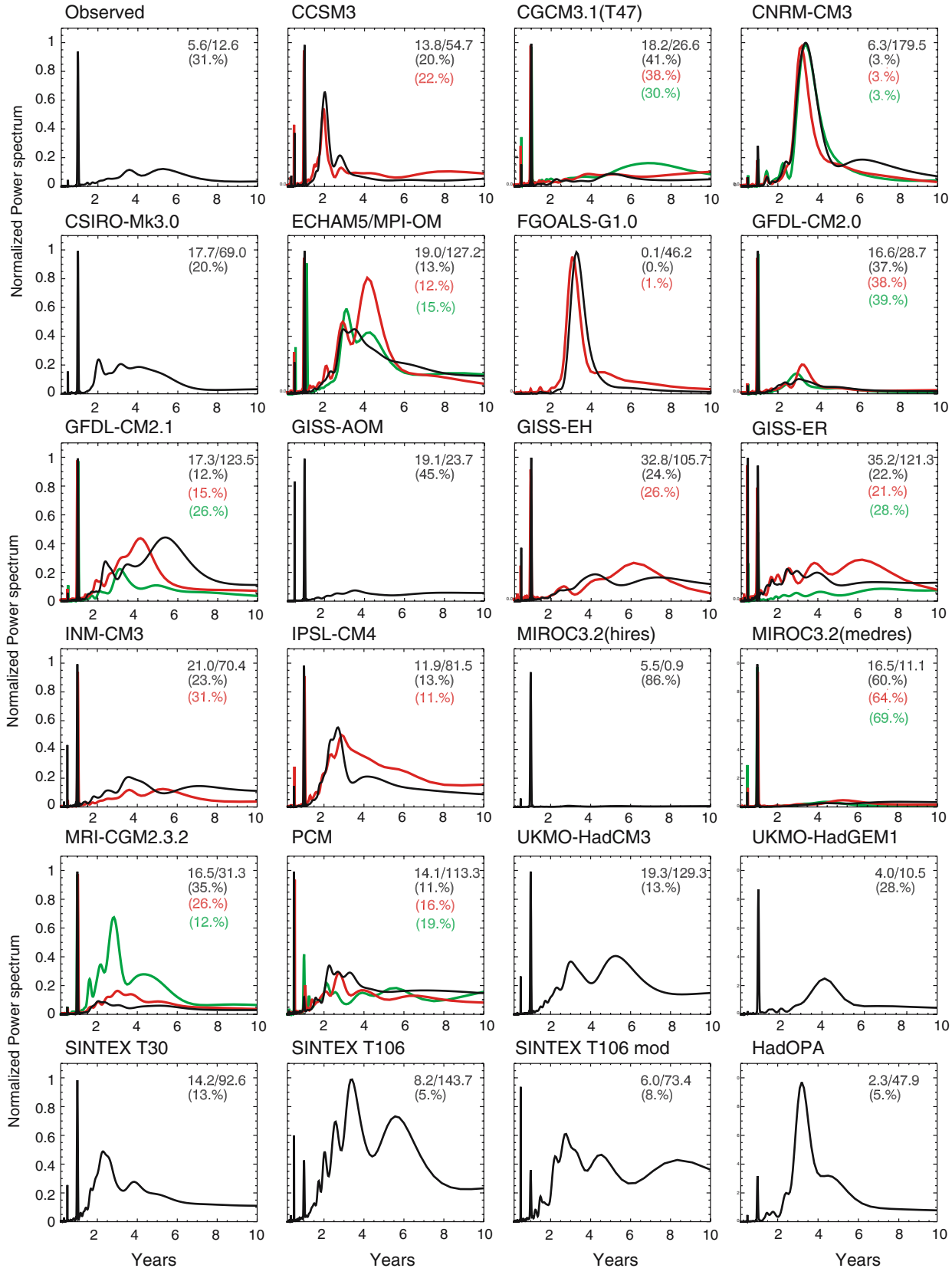

Fig. 6 Normalized power spectra of full monthly Niño3 SST for the 23 models studied, together with the available scenarios. Observation are for the HadISST1.1 dataset, years 1900–2000. Models colour code: *black* picntrl, *red* 1pctto2x (after stabilization), *green* 1pctto4x (after stabilization). The N/M values are respectively the amount of energy of the annual and semi-annual cycles and the amount of energy in the inter-annual signal for the picntrl simulations. The *value below* indicates the percentage of total spectral energy in the annual and semi-annual cycles for the available scenarios

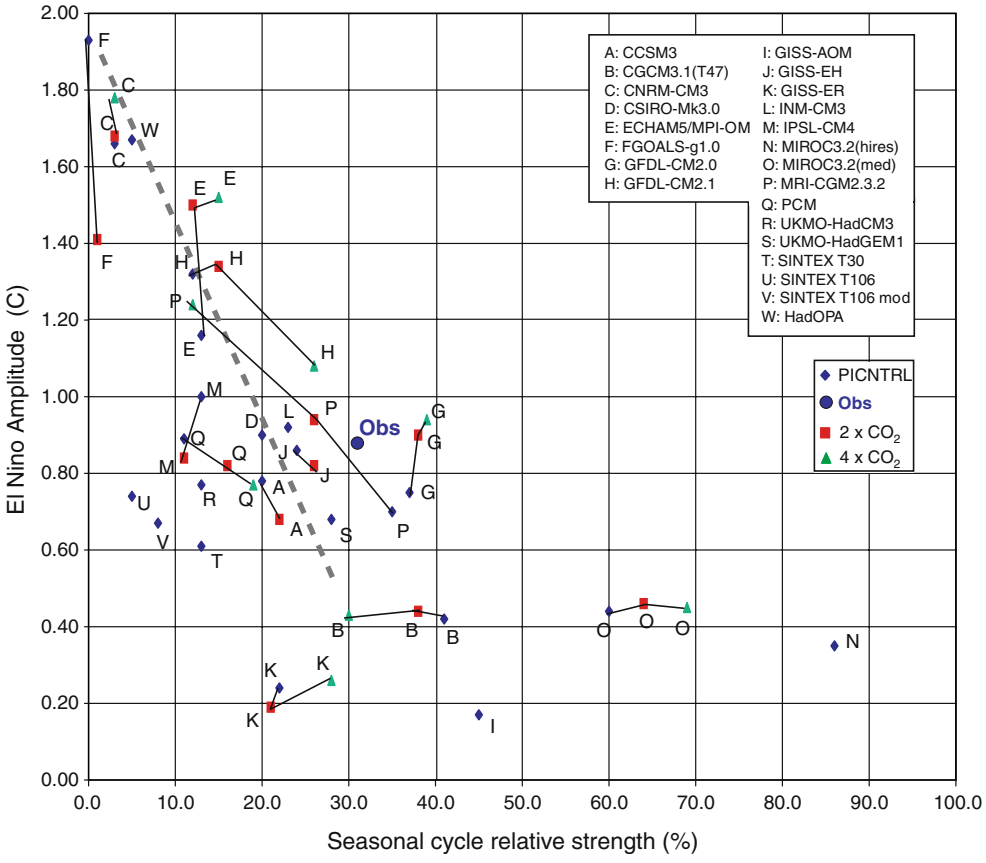

Fig. 7 Scatter plot of El Niño amplitude (°C) as a function of the seasonal cycle relative strength (%) and linear fit (*thick dashed line*, excluding models with El Niño amplitudes less than 0.5°C). *Black diamonds* picntrl, *red squares* 1pctto2x (after stabilization), *green triangles* 1pctto4x (after stabilization). The *blue circle* represents the observations. *Letters* correspond to model codes in Table 2

1995; Fedorov and Philander 2001) or using simpler models (Chang et al. 1995). When most of the energy is within the seasonal cycle, little is left for inter-annual signal and vice versa. This result can be related to the analysis above in the sense that if El Niño is defined as a disruption of the seasonal cycle, then a strong seasonal cycle is less likely to be disrupted, and vice versa. This relation holds for CO_2 scenarios as well, although the relative strength of the seasonal cycle can either increase (e.g. GFDL-CM2.1, PCM) or decrease (MRI-GCM2.3.2).

From the previous analysis, a weak seasonal cycle seems a stronger prerequisite to larger amplitude El Niño events than a low mean τ_x, even though both contribute. This result will become clearer when we analyse El Niño in terms of modes in Sect. 4.

3.4 Diagnosing a coupling strength in CGCMs

The coupling strength between the ocean and the atmosphere has been shown to be a key parameter for El Niño frequency and amplitude in simple coupled models (Zebiak and Cane 1987; Fedorov and Philander 2000; van der Vaart et al. 2000). Physically, the coupling strength measures how strongly the atmospheric winds respond to SST anomalies. In the delayed oscillator model, for example, the larger this coupling strength, the longer the El Niño period and the larger its amplitude. In coupled GCMs there is no direct, tune-able parameter for the coupling strength, but it can nevertheless vary from one model to another due to variations in the parameterizations of boundary layer, convective processes, or coupling technique, in particular. Guilyardi et al. (2004) pointed out this measure as a possible reason for the diversity of modelled El Niño in CGCMs. An interannual coupling strength (ICS) is defined here as the linear slope fit of the $\tau_x A|_{\mathrm{Nino4}} = F(\mathrm{SSTA}|_{\mathrm{Nino3}})$ Gill-type relationship, where $\tau_x A|_{\mathrm{Nino4}}$ is the monthly τ_x anomaly (with respect to the mean seasonal cycle) in the Niño4 region and $\mathrm{SSTA}|_{\mathrm{Nino3}}$ is the monthly SST anomaly in the Niño3 region (Fig. 8). This relation is a first attempt to define a standard coupling strength diagnostic in GCMs.[4] The stronger the slope, the larger the ICS, i.e. for a given SST anomaly in Niño3, the larger the τ_x anomaly in Niño4. The seasonal cycle (with mean state removed for better comparison) is added and again it is clear that the amplitude of the inter-annual variability is anti-correlated with the amplitude of the seasonal cycle. Several studies emphasise the role of the "summer" (June–November) coupling strength in El Niño growth and amplitude (Zebiak and Cane 1987; Clement et al. 1999). The summer ICS for

[4] it does not aim at representing the actual Gill relation in each CGCM (in which case, and as pointed out earlier, diagnostic regions would vary as in van Oldenborgh et al. 2005)

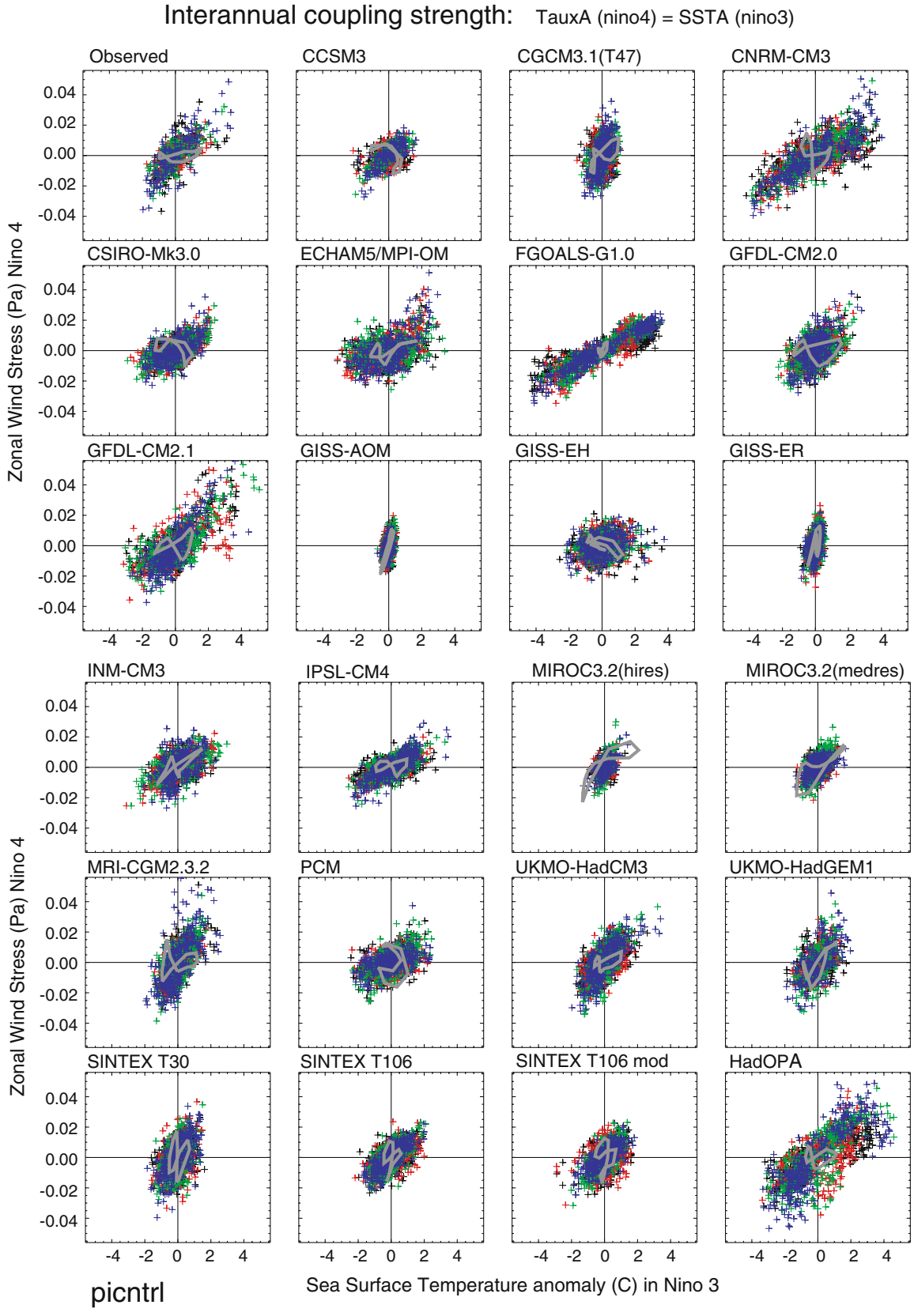

Fig. 8 The $\tau_x A|_{\text{Nino4}} = F(\text{SSTA}|_{\text{Nino3}})$ Gill-type relationship for observations and picntrl models. The linear slope fit defines the interannual coupling strength (*ICS*). Each *cross* represent a monthly value and the *colours* represent seasonal means (*black* DJF, *blue* MAM, *red* JJA, *green* SON). The *grey curves* represent the seasonal cycle of Fig. 4 with the mean state removed

models and observation has been computed and is presented in Fig. 9. Observations show three characteristics: a summer ICS value of 8.7×10^{-3} Pa/C, a larger scatter for El Niño events larger than 2°C (Fig. 8), a warm-cold asymmetry (Fig. 8).

Several—sometimes overlapping—type of modelled ICS can be distinguished: those with a weaker-than-observed ICS (e.g. FGOALS-g1.0 or IPSL-CM4), those with a larger-than-observed ICS (CGCM3.1(T47) or MRI-CGM2.3.2), those with no clear slope (e.g. GISS-EH or PCM), those with symmetric warm-cold patterns (e.g. SINTEX models). Some models do have a more or less correct ICS together with the warm-cold asymmetry and the larger scatter behaviour for large events (ECHAM5/MPI-OM, GFDL-CM2.0, GFDL-CM2.1, UKMO-HadCM3).

For most models, the ICS in 1pctto2x and 1pctto4x does not exhibit much change except for a few models that experience strong reduction with increasing CO_2 (MIROC3.2 (medres), MRI-CGM2.3.2, PCM) (Fig. 9).

Relating the dominant El Niño frequency with the ICS in an attempt to compare with simpler models results (larger coupling strength leads to longer period El Niño events) is not very conclusive (Fig. 10). If we eliminate the ''somewhat exotic'' models (GISS models, flux corrected MRI-GCM2.3.2, MIROC3.2(hires) with extreme seasonal cycle), the remaining subset of CGCMs is in closer agreement with the results of simpler models.

4 SST versus thermocline mode

4.1 Diagnosing an El Niño mode in GCMs

In order to further describe the mechanisms responsible for the relations described above, we now assess the modelled El Niño in terms of modes. We consider the two types of modes that can give rise to El Niño: the S-mode, resulting from local SST–winds interactions in the central-east Pacific, implying surface east to west propagation of SST anomalies and low amplitude events with a 2–3 years frequency, as evidenced in observations for the 1948–1976 period[5] and the T-mode, resulting from remote winds–thermocline feedbacks involving the west Pacific, implying subsurface west to east propagation and large amplitude events with 4-years frequency, as evidenced in observations for the post-1976 period with the 1982/83 and 1997/98 events. Many analysis techniques have been proposed to diagnose these modes. As no thermocline data is available in the IPCC database for the scenarios used here, we choose to diagnose these modes in the CGCMs via the direction of SST anomalies propagation. We apply the simple and elegant technique proposed by Trenberth and Stepaniak (2001) by lag-correlating the Trans Nino Index (or TNI, which measures the east–west zonal gradient of SST by taking the difference between the normalized SSTA in the Niño1 + 2 region in the east Pacific and the normalized SSTA in the Niño4 region in the central west Pacific) and the normalized Niño3 SSTA. It was checked for all models that the direction of propagation diagnosed with this technique agrees with the direction of propagation as qualitatively seen on equatorial hovmoellers of SST.

Figure 11 displays this lag-correlation (±20 months lags and using a running time-window of 12 years) together with the normalized Niño3 SSTA time serie for observations and a few typical models. A negative correlation for positive lags mean that TNI is leading Niño3 SSTA (i.e. S-mode) and a positive correlation for positive lags mean the opposite (i.e. T-mode). In the observations, the 1948–1976 dominant westward S-mode (with lower amplitude El Niño events) and the post-1976 dominant eastward T-mode (with larger El Niño events) are well captured. Because of the co-existence of these two modes, Fedorov and Philander (2001) and Burgers and van Oldenborgh (2003) describe El Niño in the observations as driven by a hybrid mode. The models shown exhibit all three types of modes: S-mode (CNRM-CM3, FGOALS.g1.0), T-mode (GFDL-CM2.1, HadOPA) or hybrid (ECHAM5/MPI-OM, IPSL-CM4, UKMO-HadCM3). Note that models exhibiting a dominant T-mode also have periods of S-mode (like years 20–30 in GFDL-CM2.1 or 70–80 in HadOPA) whereas the reverse is not systematic. Like in observations, periods of T-mode (or reduced S-mode) in models correspond to large El Niño events (years 185, 230 and 275 in ECHAM5/MPI-OM, years 100 and 120 for IPSL-CM4 or years 65, 180, 220 in UKMO-HadCM3 for example).

To assess the mode type for all models and scenarios, the time mean lag-correlation is shown in Fig. 12, together with ±1 standard deviation. A small standard deviation for months +1 to +12 (usually associated with an S-mode) means that the mode is very stable (CNRM-CM3, CSIRO-Mk3.0, FGOALS-g1.0) whereas a large one can mean the mode may change with time (if the lag-correlation for months +1 to +12 changes sign for instance) (Observations, ECHAM5/MPI-OM, GFDL-CM2.0, GFDL-CM2.1, MRI-CGM2.3.2, UKMO-HadCM3, HadOPA). Models exhibiting such a change of mode are of particular interest as they most likely have the basic mechanisms to lead to El Niño characteristics changes in different climates. For that purpose and to increase the data base for further analysis, a proxy to the 1pctto2x for UKMO-HadCM3 is taken as the stabilized period of the SRES1B scenario (no such scenario is available yet for the HadOPA model).

4.2 Mode evolution in scenarios

As evidence by the shift towards positive correlation for lags [+1, +12] from picntrl to 1pctto2x and 1pctto4x, a

[5]The quality of the SST data prior to 1948 is not sufficient to assess such a relationship.

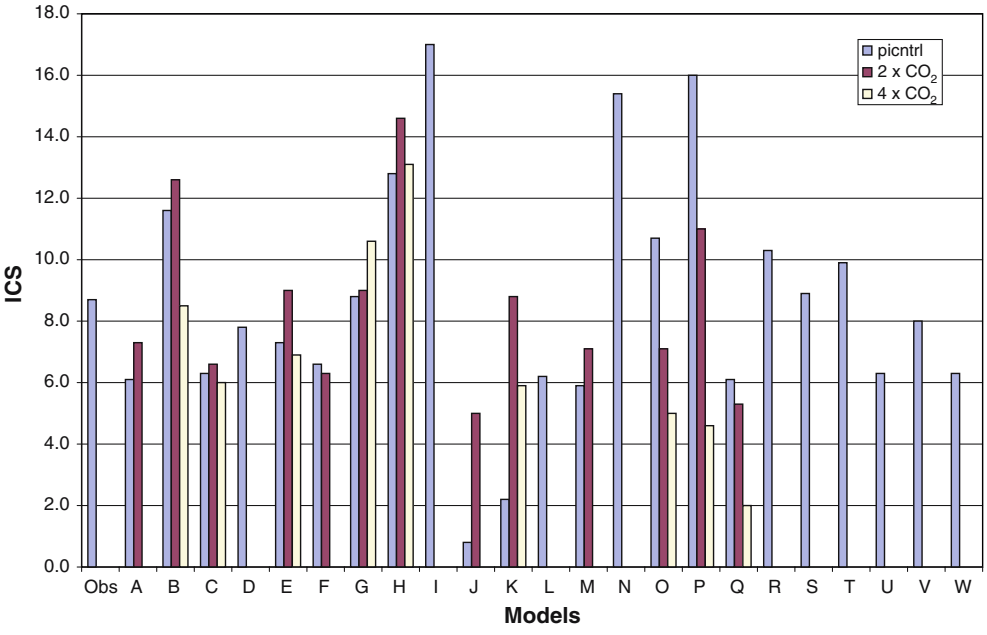

Fig. 9 Summer (June–Nov.) inter-annual coupling strength (*ICS*) for the observation and the models for picntrl, 1pctto2x and 1pctto4× (10^{-3} Pa/C)

number of models exhibit a mode shift towards a T-mode (either from S-mode to hybrid or hybrid to T-mode) in the increased GHG scenarios. To further assess this relation, the El Niño amplitude change as a function of the mode type (average correlation for lags [+1, +12]) is shown in Fig. 13. The models that exhibit the largest El Niño amplitude change are those that undergo a mode shift from a S-mode towards a T-mode (MRI-GCM2.3.2, ECHAM5/MPI-OM, GFDL-CM2.0, and to a lesser extend, MIROC3.2(medres) and UKMO-Had-

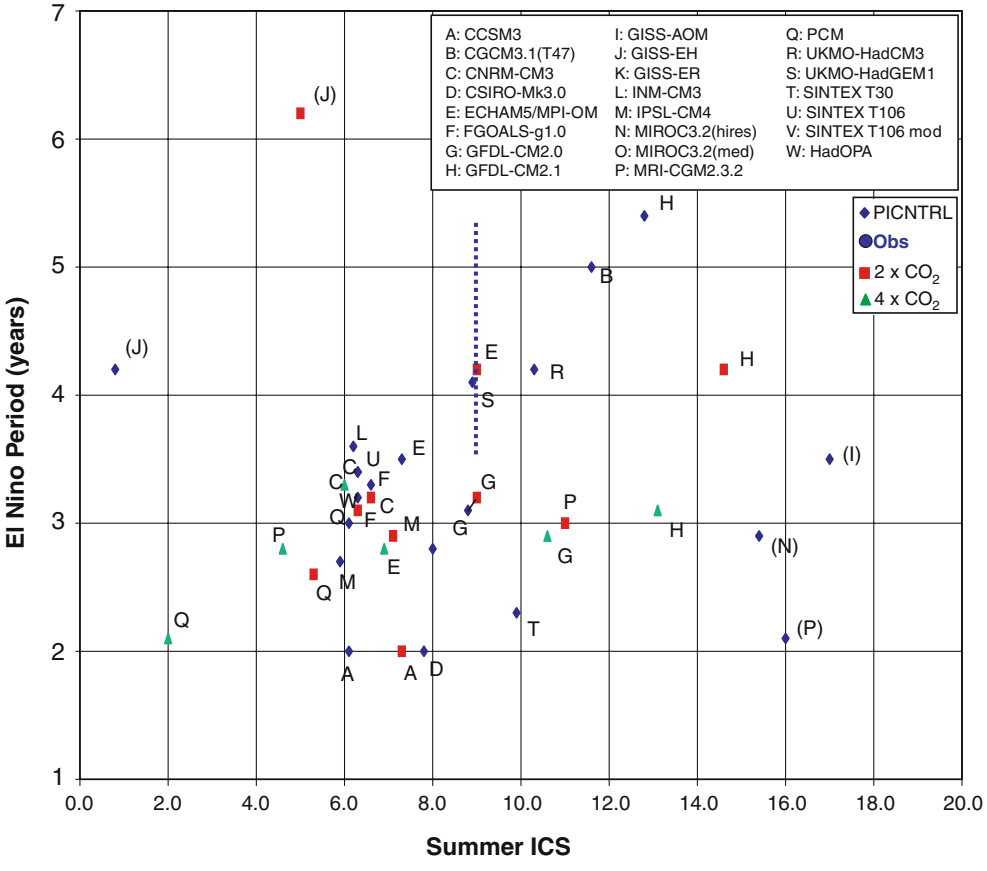

Fig. 10 El Niño period (in years) as a function of the summer (June-Nov) inter-annual coupling strength (ICS, in 10^{-3} Pa/C) for the models. *Black diamonds* picntrl, *red squares* 1pctto2x (after stabilization), *green triangles* 1pctto4x (after stabilization). The *blue dotted line* represents the range of observations. Models in parenthesis are those referred as "exotic" in the text

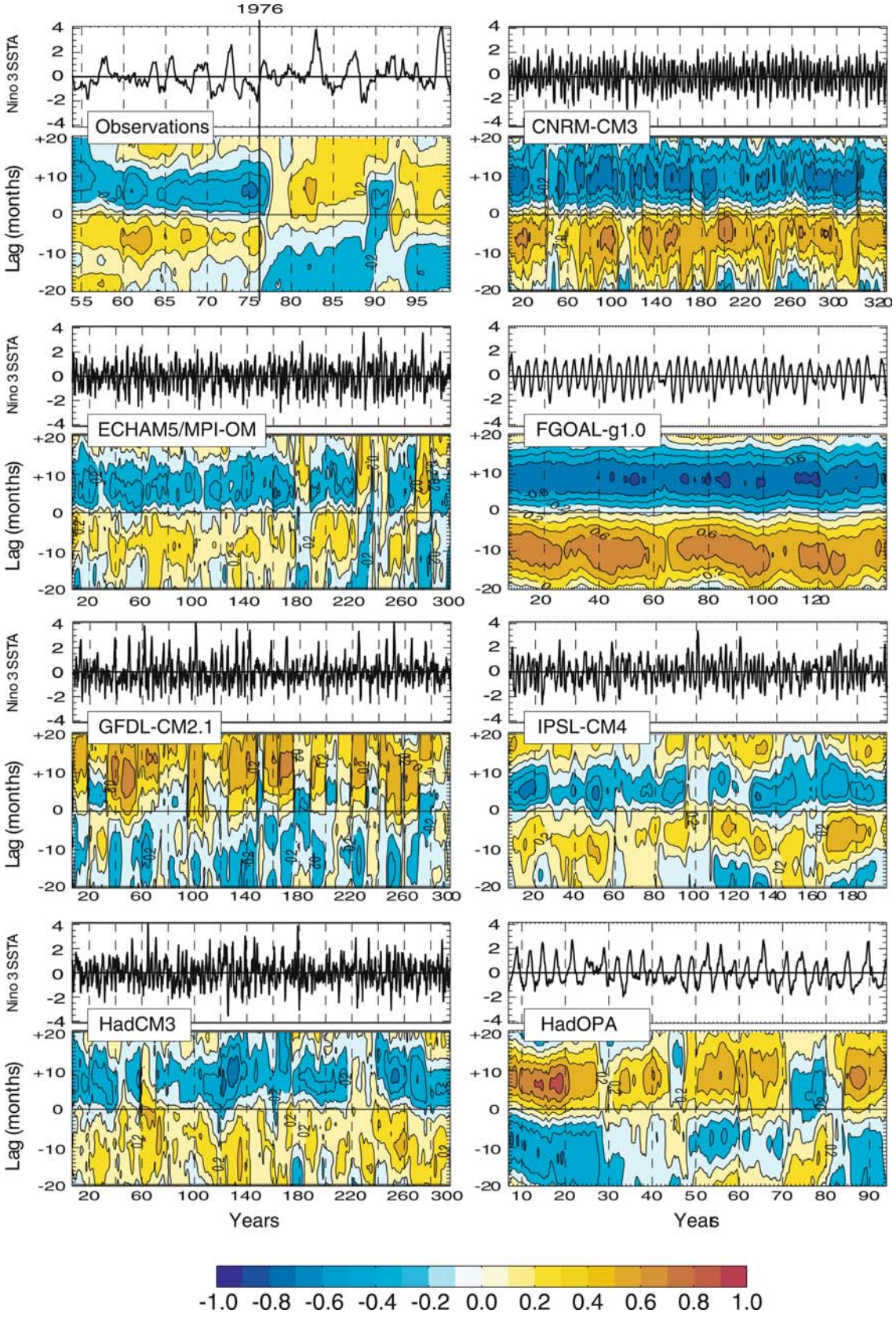

Fig. 11 Lag-correlation of the Trans Niño Index (*TNI*) with the normalized Niño3 SSTA for observations and a few typical models. The normalized Niño3 SSTA curve is also shown above. Diagnostics are done using a 12 years running window. A positive Correlation (*yellow to red*) means Niño3 SST is leading the TNI and the direction of equatorial SST anomaly propagation is west to east

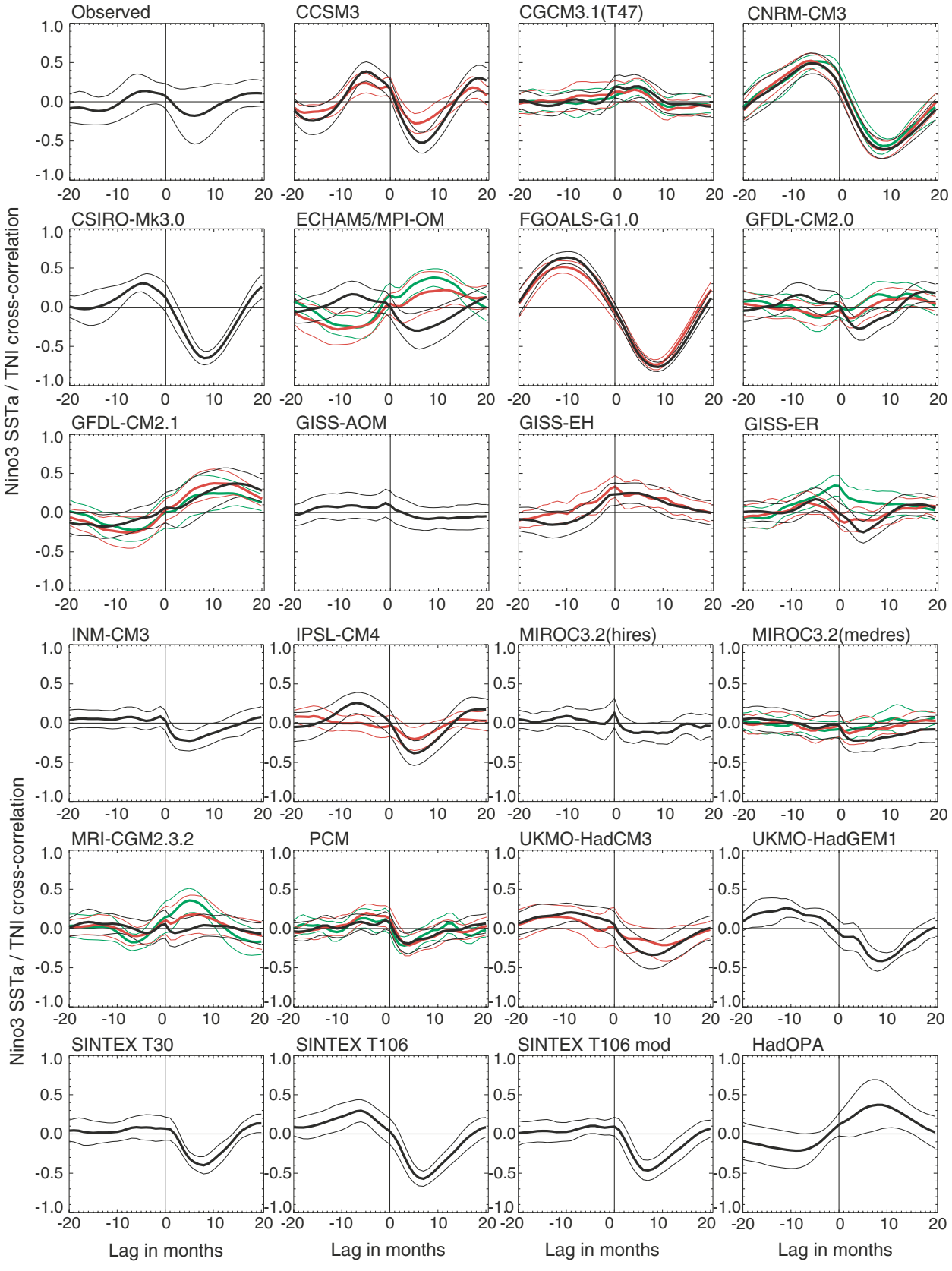

Fig. 12 The time mean lag-correlation of TNI and Niño3 SSTA (*thick line*), together with ±1 standard deviation (*thin lines*) for observations and all models and scenarios. *Black* picntrl, *red* 1pctto2x (after stabilization), *green* 1pctto4x (after stabilization)

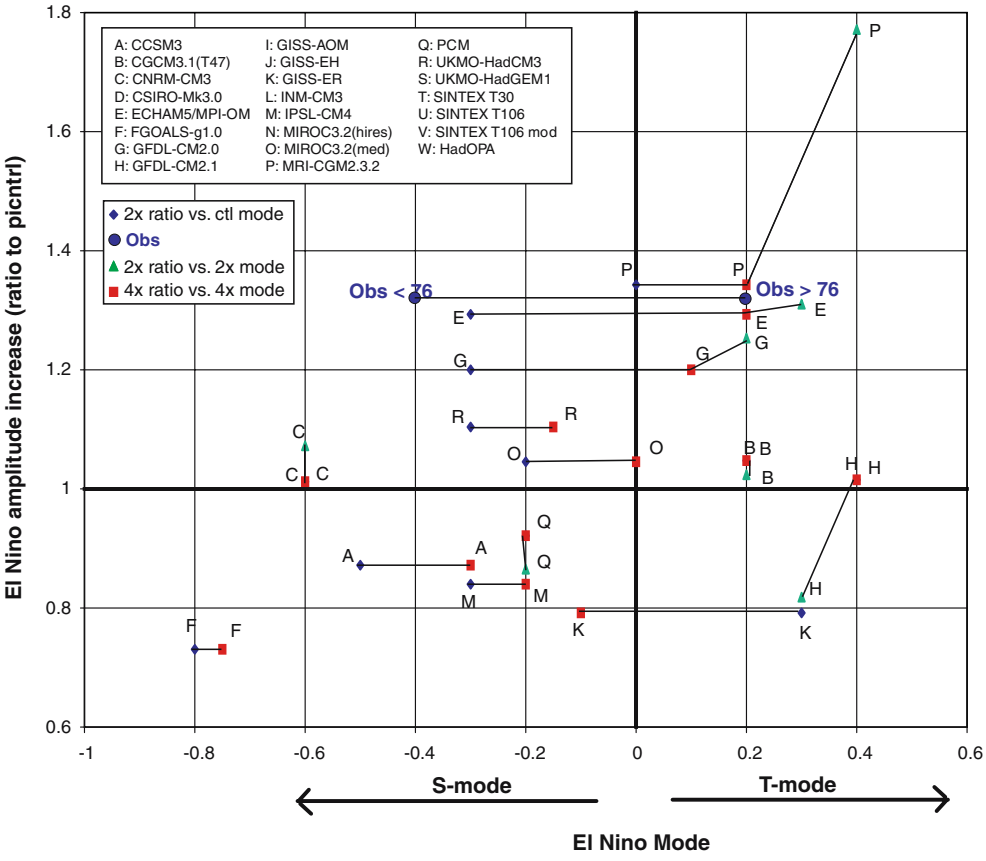

Fig. 13 El Niño amplitude change from picntrl to 1pctto2x and 1pctto4x as a function of El Niño mode as defined in the text

CM3). The GFDL-CM2.1 model, which already has a strong T-mode for picntrl, does not show any El Niño amplitude increase for 1pctto2x, and exhibits a decreased El Niño amplitude for 1pctto4x, with a related decrease in the strength of the T-mode.

4.3 Mode and frequency

The relation between El Niño mode and El Niño frequency as defined earlier is presented in Fig. 14. Although there is no clear relationship, the simulations that exhibit a T-mode tend to have a lower frequency El Niño amplitude (2.8–5.4 years against 2–4.2 for the S-mode) together with a larger summer ICS (not shown), in agreement with simpler model results (Zebiak and Cane 1987; Fedorov and Philander 2001). No clear indication emerges on how the frequency evolves from picntrl to 1pctto2x and 1pctto4x, even if only the models that exhibit a mode change (as defined above) are retained.

4.4 Mode, mean state and seasonal cycle

Several studies relate the El Niño mode to the mean state in the tropical Pacific, in particular to the strength of the mean winds (Fedorov and Philander 2001; Burgers and van Oldenborgh 2003). No such clear relation is found here. One could relate the stronger-than-observed winds in most models to the dominant S-mode exhibited by many models, but some T-mode models also have strong trade winds. Note though that most of the models that do exhibit the mode shift in the scenario simulation (as discussed above) have a moderate seasonal cycle relative strength (but maybe GFDL-CM2.1, Fig. 7). Indeed, the T-mode involves equatorial Kelvin waves which need a seasonal relaxation of the trade winds at the end of the winter to propagate heat anomalies from west to east (Vialard et al. 2001). Subsurface data will most likely need to be analysed to draw further conclusions on this specific issue.

5 Summary and discussion

In this study, the relation between the equatorial Pacific mean state and seasonal cycle and El Niño characteristics is analysed in 23 coupled ocean–atmosphere GCMs and three types of IPCC AR4 scenarios (pre-industrial control, stabilized double and quadruple CO_2). Overall, the number of models that correctly represent the main features of the equatorial climate (in particular in SST) is much higher than previous inter-comparisons. Several bias are still systematic like both too strong mean trades winds and seasonal cycle. Because of the diversity of modelled mean state and seasonal cycle, an attempt is made to identify relationships between these and El

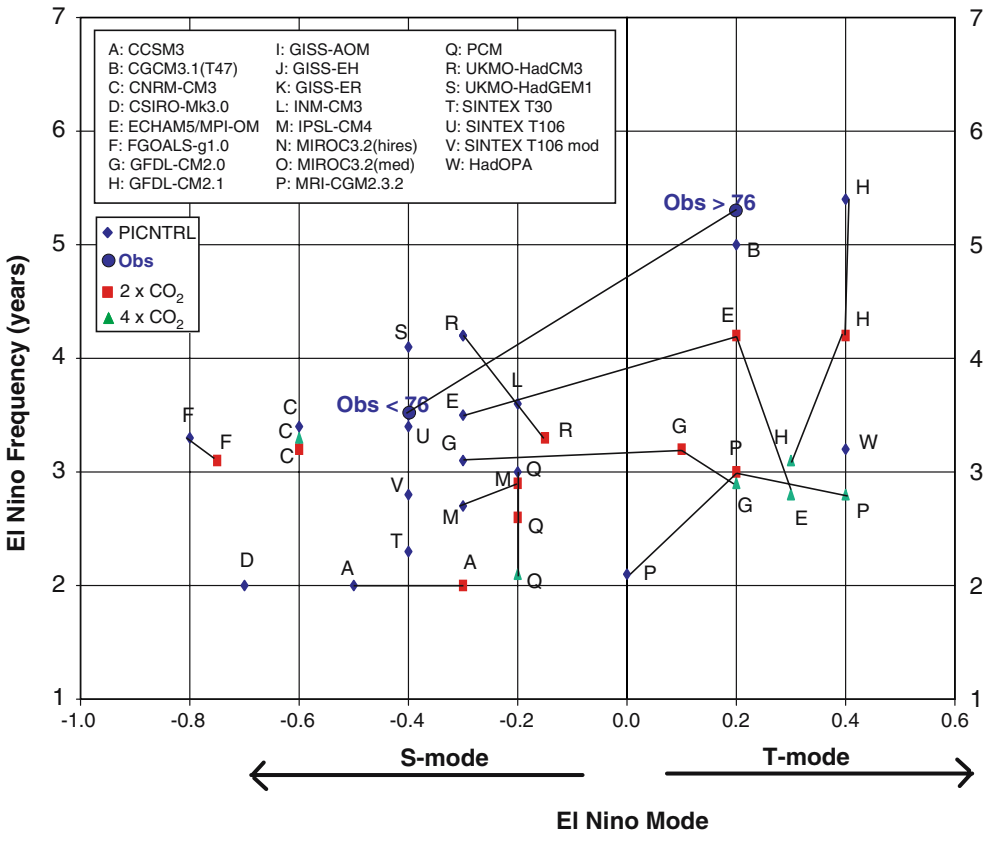

Fig. 14 El Niño frequency as a function of El Niño mode (see text)

Niño characteristics, as previously done in theoretical frameworks, or in observations.

Major results include:

- El Niño amplitude is shown to be an inverse function of the mean trade winds. This agrees with the observed shift of 1976 and with theoretical studies.
- El Niño amplitude is shown to be an inverse function of the relative strength of the seasonal cycle. This agrees as well with the few theoretical studies available, either using simple models or observations. When most of the energy is within the seasonal cycle, little is left for inter-annual signal and vice versa. As El Niño is defined as a disruption of the seasonal cycle, then a strong seasonal cycle is less likely to be disrupted, and vice versa.
- An ICS is defined and, for a subset of models, its relation with the modelled El Niño frequency somewhat follows that predicted by theoretical models, i.e. that the larger the coupling strength, the lower the El Niño frequency.
- The modelled El Niño are then assessed in term of the two modes described in previous work: the S-mode implying surface east to west propagation of equatorial SST anomalies and low amplitude events with a 2–3 years frequency, as evidenced in observations for the pre-1976 period and the T-mode, resulting from remote winds–thermocline feedbacks involving the west Pacific, implying subsurface west to east propagation and large amplitude events with 4–5 years frequency, as evidenced in observations for the post-1976 period. It is shown that most models are locked into an S-mode (probably due to the strong trade winds) and that a few models exhibit an hybrid mode, like in observations.
- Although there is no clear relationship between the El Niño mode and the El Niño frequency, the models that exhibit a T-mode tend to have a lower frequency El Niño than the others, as predicted by theoretical studies.
- Most of these relationships, first established for the pre-industrial simulations, hold for the double and quadruple CO_2 scenarios. A recurrent exception is the flux corrected MRI-CGM2.3.2 model.
- The models that exhibit the largest El Niño amplitude change in these GHG scenarios are those that exhibit a mode change towards a T-mode (either from S-mode to hybrid or hybrid to T-mode). This is all the more interesting as the 1976 climate shift in the tropical Pacific also involved such a mode shift and several studies suggested this shift was climate change related (although this issue it still hotly debated as it might also be a decadal variability signal—Trenberth and Hurrell 1994). In many respects, these models are also among those that best simulate the tropical Pacific climatology (ECHAM5/MPI-OM, GFDL-CM2.0, GFDL-CM2.1, MRI-CGM2.3.2, UKMO-HadCM3). This suggest the likelihood of increased El Niño amplitude in a warmer climate, when compared

to the conclusions of other related studies (Collins and the CMIP Modelling Groups 2005; van Oldenborgh et al. 2005; Merryfield 2005), though there is considerable spread of El Niño behaviour among the models and the changes in the subsurface thermocline properties that may be important for El Niño change could not be assessed.

These results are encouraging in that several basic El Niño–mean state–seasonal cycle relationships proposed by either theory or analysis of observations seem to be reproduced by CGCMs. This is especially true for the amplitude of El Niño and is less clear for its frequency. Even though the mode analysis performed captures the basic El Niño dynamics, this study did not cover all aspects of modelled El Niño and should be pursued. In addition to the key subsurface analysis, off-equatorial processes, which have been shown to play a central role in El Niño turn about (Chang 1996; Guilyardi et al. 2003; Vecchi and Harrison 2003; Spencer 2005; van Oldenborgh et al. 2005) should be assessed. The causes of the very different modelled seasonal cycle was not discussed and should also be addressed. Only stabilized scenarios were analysed here, which represent best case scenarios for pulling out El Niño change and justifies performing such idealized simulations. Detecting El Niño change in transient simulations (which is what the real system is) is more difficult due to the signal to noise problems involved with a slowly varying forcing and inherent natural (decadal) variability.

Acknowledgments I am grateful to Pascale Delecluse, Julia Slingo, Matthieu Lengaigne, Alexey Fedorov, Jo Brown, Krishna AchutaRao and Pascale Braconnot for fruitful discussions, to Pascal Terray for help with the statistical computations, and to Jerry Meehl and Geert Jan van Oldenborgh for improving the original manuscript. I acknowledge the international modelling groups for providing their data for analysis, the Program for Climate Model Diagnosis and Intercomparison (PCMDI) for collecting and archiving the model data, the JSC/CLIVAR Working Group on Coupled Modelling (WGCM) and their Coupled Model Intercomparison Project (CMIP) and Climate Simulation Panel for organizing the model data analysis activity, and the IPCC WG1 TSU for technical support. The IPCC Data Archive at Lawrence Livermore National Laboratory is supported by the Office of Science, U.S. Department of Energy. The support of the European Union's Framework Programme VI via the DYNAMITE project (contract #003903) is also acknowledged. NCEP Reanalysis data was provided by the NOAA-CIRES Climate Diagnostics Center, Boulder, Colorado, USA, from their Web site at http://www.cdc.noaa.gov/.

References

AchutaRao K, Sperber K (2002) Simulation of the El Niño Southern Oscillation: results from the coupled model intercomparison project. Clim Dyn 19:191–209

AchutaRao K, Sperber K (2005) ENSO simulations in coupled ocean–atmosphere models: are the current models better? Clim Dyn (submitted)

Burgers G, van Oldenborgh GJ (2003) On the impact of local feedbacks in the central Pacific on the ENSO cycle. J Clim 16:2396–2407

Chang P (1996) The role of the dynamic ocean–atmosphere interactions in tropical seasonal cycle. J Clim 9:2973–2985

Chang P, Ji L, Wang B, Li T (1995) Interactions between the seasonal cycle and el niño-southern oscillation in an intermediate coupled ocean–atmosphere model. J Atmos Sci 52:2353–2372

Clement A, Seager R, Cane M (1999) Orbital controls on the EL Niño/Southern Oscillation and the tropical climate. Paleoceanog 14:441–456

Clement A, Seager R, Cane M (2000) Suppression of El Niño during the mid-Holocene by changes in the Earth's orbit. Paleoceanog 15:731–737

Cobb KM, Charles C, Cheng H, Edwards R (2003) El Niño/southern oscillation and tropical pacific climate during last millenium. Nature 424:271–276

Collins M (2000a) The El Niño-southern oscillation in the second hadley centre coupled model and its response to greenhouse warming. J Clim 13:1299–1312

Collins M (2000b) Uncertainties in the reponse of ENSO to greenhouse warming. Geophys Res Lett 27:3509–3513

Collins M, The CMIP Modelling Groups (2005) El Niño- or La Niña-like climate change? Clim Dyn 24:89–104

Davey M, Huddleston M, Sperber K et al (2001) STOIC: a study of coupled model climatology and variability in tropical ocean regions. Clim Dyn 18:403–420

Delecluse P, Davey M, Kitamura Y, Philander S, Suarez M, Bengtsson L (1998) TOGA review paper: coupled general circulation modeling of the tropical Pacific. J Geophys Res 103:14357–14373

Dijkstra H, Neelin D (1995) Ocean–atmosphere interaction and the Tropical Climatology. Part II: why the pacific cold tongue is in the east. J Clim 8:1343–1359

Fedorov AV, Philander SG (2000) Is El Niño changing? Science 288:1997–2002

Fedorov AV, Philander SG (2001) A stability analysis of tropical ocean–atmosphere interactions: bridging measurements and theory for El Niño. J Clim 14:3086–3101

Gu D, Philander SG (1995) Secular changes of annual and interannual variability in the tropics during the past century. J Clim 8:864–876

Guilderson TP, Schrag DP (1998) Abrupt shift in subsurface temperatures in the tropical pacific associated with changes in El Niño. Science 281:240–243

Guilyardi E, Delecluse P, Gualdi S, Navarra A (2003) Mechanisms for ENSO phase change in a coupled GCM. J Clim 16:1141–1158

Guilyardi E, Gualdi S, Slingo JM, Navarra A, Delecluse P, Cole J, Madec G, Roberts M, Latif M, Terray L (2004) Representing El Niño in coupled ocean–atmosphere GCMs: the dominant role of the atmospheric component. J Clim 17:4623–4629

Jin F, Neelin J, Ghil M (1994) El Nino on the devil's staircase: Annual subharmonic steps to chaos. Science 264:70–72

Karspeck A, Cane M (2002) Tropical Pacific 1976/77 climate shift in a linear, wind-driven model. J Phys Oceanogr 32:2350–2360

Knutson T, Manabe S (1998) Model assessment of decadal variability and trends in the tropical Pacific Ocean. J Clim 11:2273–2296

Latif M, Sperber K et al (2001) ENSIP: the El Niño simulation intercomparison project. Clim Dyn 18:255–276

Li T, Philander G (1996) On the annual cycle in the eastern equatorial Pacific. J Clim 9:2986–2998

Meehl GA, Branstator G, Washington W (1993) Tropical Pacific interannual variability and CO_2 climate change. J Clim 6:42–63

Meehl GA, Teng H, Branstator G (2005) Future changes of in two global coupled climate models. Clim Dyn (submitted)

Merryfield WJ (2005) Changes to ENSO under CO2 doubling in the IPCC AR4 coupled climate models. J Clim (submitted)

Neelin J, Battisti D, Hirst A, Jin F, Yamagata YWT, Zebiak S (1998) ENSO theory. J Geophys Res 103:14261–14290

Nigam S, Chao Y (1996) Evolution dynamics of tropical ocean–atmosphere annual cycle variability. J Clim 9:3187–3205

Rayner N, Parker D, Horton E, Folland C, Alexander L, Rowell D, Kent EC, Kaplan A (2003) Global analyses of sea surface

temperature, sea ice, and night marine air temperature since the late nineteenth century. J Geophys Res 108:4407. DOI 10.1029/2002JD002670

Spencer H (2005) Role of the atmosphere in the seasonal phase locking of El Nino. Geophys Res Lett (submitted)

Tett S (1995) Simulation of El Niño/southern oscillation like variability in a global AOGCM and ifs reponse to CO_2 increase. J Clim 8:1473–1502

Timmermann A, Jin F, Collins M (2004) Intensification of the annual cycle in the tropical Pacific due to greenhouse warming. Geophys Res Lett 31:12208

Timmermann A, Oberhuber J, Bacher A, Esch M, Latif M (1999) Increased El Niño frequency in a climate model forced by future greenhouse warming. Nature 398:694–696

Trenberth KE, Hurrell J (1994) Decadal atmosphere–ocean variations in the Pacific. Clim Dyn 9:303–319

Trenberth KE, Stepaniak DP (2001) Indices of El Niño evolution. J Clim 14:1697–1701

Tudhope A et al (2001) Variability in the El Niño-southern oscillation through a glacial-interglacial cycle. Science 291:1511–1517

Tziperman E, Stone L, Cane MA, Jarosh H (1994) El Niño chaos: overlapping of resonances between the seasonal cycle and the Pacific ocean–atmosphere oscillator. Science 264:72–74

Tziperman E, Zebial SE, Cane MA (1997) Mechanisms of seasonal–ENSO interaction. J Atmos Sci 54:61–71

Urban FE, Cole JE, Overpeck JT (2000) Influence of mean climate change on climate variability from a 155-year tropical Pacific coral record. Nature 407:989–993

van der Vaart P, Dijkstra HA, Jin FF (2000) The Pacific cold tongue and the ENSO mode: a unified theory within the Zebiak-Cane model. J Atmos Sci 57:967–988

van Oldenborgh G, Philip S, Collins M (2005) El Niño in a changing climate: a multi-model study. Ocean Model (submitted)

Vecchi G, Harrison D (2003) On the termination of the 2002–03 El Nino event. Geophys Res Lett 30(18):1964. DOI 10.1029/2003GL017564

Vialard J, Menkes C, Boulanger J, Guilyardiand E, Delecluse P, McPhaden MJ (2001) Oceanic mechanisms driving the SST during the 1997–98 El Niño. J Phys Oceanogr 31:1649–1675

Wang B, An S (2002) A mechanism for decadal changes of ENSO behaviour: roles of background wind changes. Clim Dyn 18:475–486

Wang C, Picaut J (2004) Understanding ENSO Physics—A Review. In: Wang C, Xie S-P, Carton JA (eds) Earth's climate: the ocean–atmosphere interaction Geophysical Monograph Series. AGU, Washington D.C., pp 21–48

Zebiak SE, Cane MA (1987) A model El Niño-Southern Oscillation. Mon Wea Rev 115:2262–2278

Zelle H, van Oldenborgh G, Dijkstra H (2005) El Nino and greenhouse warming: results from ensemble simulations with the NCAR CCSM. J Clim (submitted)